Onset of convection with fluid compressibility and interface movement

Cite as: Phys. Fluids **25**, 094105 (2013); https://doi.org/10.1063/1.4821743
Submitted: 28 June 2013 . Accepted: 05 September 2013 . Published Online: 25 September 2013

Philip C. Myint, and Abbas Firoozabadi

PHYSICS OF FLUIDS **25**, 094105 (2013)

Onset of convection with fluid compressibility and interface movement

Philip C. Myint[1,2,a)] and Abbas Firoozabadi[1,3,b)]
[1]*Department of Chemical and Environmental Engineering, Yale University, 9 Hillhouse Avenue, New Haven, Connecticut 06511, USA*
[2]*Atmospheric, Earth, and Energy Division, Lawrence Livermore National Laboratory, Livermore, California 94550, USA*
[3]*Reservoir Engineering Research Institute, Palo Alto, California 94301, USA*

(Received 28 June 2013; accepted 5 September 2013; published online 25 September 2013)

The density increase from carbon dioxide (CO_2) dissolution in water or hydrocarbons creates buoyancy-driven instabilities that may lead to the onset of convection. The convection is important for both CO_2 sequestration in deep saline aquifers and CO_2 improved oil recovery from hydrocarbon reservoirs. We perform linear stability analyses to study the effect of fluid compressibility and interface movement on the onset of buoyancy-driven convection in porous media. Compressibility relates to a non-zero divergence of the velocity field. The interface between the CO_2 phase and the aqueous or hydrocarbon phase moves with time as a result of the volume change that occurs upon CO_2 dissolution. Previous stability analyses have neglected these two aspects by assuming that the aqueous or hydrocarbon phase is incompressible and that the interface remains fixed in position. The stability analyses are used to compute two key quantities: (1) the critical time and (2) the critical wavenumber. Our results indicate that compressibility has a negligible effect on the critical time and the critical wavenumber in CO_2-water mixtures. We use thermodynamics to derive an expression which shows that the two opposing physical processes which contribute to the divergence are comparable in magnitude and largely cancel each other. This result explains why compressibility does not significantly affect the onset, and it also demonstrates the link between compressibility and the volume change that causes movement of the interface. Compared to when the interface is fixed in position, a moving interface in CO_2-water mixtures may reduce the critical time by up to around 10%, which can be significant in low permeability formations. The decrease in the critical time due to interface movement may be much more pronounced in hydrocarbons than in water. This could have important implications for CO_2 improved oil recovery. [http://dx.doi.org/10.1063/1.4821743]

I. INTRODUCTION

Global energy demand from fossil fuels is expected to remain over 70% in the coming decades, despite considerable efforts to develop alternative energy sources.[1] Combustion of fossil fuels contributes to rising atmospheric carbon dioxide (CO_2) levels that have been linked to climate change. Subsurface CO_2 injection can help society meet its high demand for fossil fuels and reduce atmospheric CO_2 levels. Carbon dioxide has been employed for over four decades in improved oil recovery.[2,3] Dissolution of CO_2 in oil may reduce the viscosity by over an order of magnitude and may increase the volume of the resulting mixture by up to 60%. The volume expansion helps to expel the oil from smaller porous cavities. Within the past two decades, CO_2 injection for sequestration in deep saline aquifers has received considerable attention as a promising way to reduce atmospheric

a)Electronic mail: philip.myint@yale.edu
b)Electronic mail: abbas.firoozabadi@yale.edu

CO_2 levels.[4–6] This process involves capturing CO_2 emissions from stationary sources, such as power plants, and storing the CO_2 by dissolving it in the aqueous phase that resides in the aquifers. The CO_2 is usually injected at supercritical conditions and forms a free phase because CO_2 is only partially miscible with the *in situ* aqueous or hydrocarbon phase. We refer to the aqueous or hydrocarbon phase collectively as the liquid phase. The CO_2 phase is typically lighter than the liquid phase, and it initially mixes with the underlying liquid only by diffusion.

Carbon dioxide is the only common atmospheric gas that increases the density of hydrocarbons upon dissolution,[7] and one of the few that increases the density of water.[8] The density increase creates an unstable situation where heavier, CO_2-dissolved fluid lies on top of lighter fluid. The instabilities may lead to the onset of buoyancy-driven convection in the liquid phase. Convection is of great interest because it strongly enhances the CO_2 dissolution rate over diffusion alone. In this way, it increases the efficiency of improved oil recovery processes. However, the convection may also lead to earlier appearance of CO_2 in the production well, which is an undesirable consequence that must be monitored in field-scale operations.[9,10] Convection not only increases the storage efficiency of CO_2 sequestration, it also has implications for the long-term storage security of the CO_2. The enhanced dissolution of CO_2 into the aqueous phase reduces the pressure buildup in the free CO_2 phase. The pressure reduction makes it less likely that the cap rock enclosing the aquifer will fracture, which lowers the risk of CO_2 leakage back into the atmosphere. Thus, convection is important for both CO_2 improved recovery and CO_2 sequestration, and it is of interest to determine the conditions under which the instabilities may lead to the onset of convection in the liquid phase.

Several authors have performed a linear stability analysis to theoretically predict the onset of buoyancy-driven convection in the context of CO_2 sequestration.[11–16] Their work has been extended to include features such as hydrodynamic dispersion,[17] temperature gradients,[18,19] chemical reactions,[20,21] and permeability anisotropy.[22–24] The state of the system before the onset of convection, when CO_2 is transported through the liquid phase only by diffusion, is referred to as the base state. The stability analysis is a semi-analytical method that introduces small wave-like perturbations to the base state in order to determine the conditions under which the base state becomes unstable. The stability analysis is used to calculate two key quantities: (1) the critical time and (2) the critical wavenumber. Onset of convection occurs at the critical time, which represents the first instance when the base state becomes unstable. The critical wavenumber characterizes the most unstable perturbation mode. There have also been a number of numerical simulations[25–29] and laboratory-scale experiments[30–32] regarding CO_2 sequestration. However, simulations and experiments focus on the time when the average CO_2 concentration in the liquid phase begins to deviate from the diffusion-only profile. This time may be quite distinct from the critical time and is an aspect of convection that is not examined by the stability analysis, which investigates only the onset of instability.[16,24,29]

The aforementioned linear stability analyses have employed a common set of assumptions. For example, various authors consider a situation where enough CO_2 has been injected into the subsurface to form a reservoir that keeps the interface between the CO_2 phase and the liquid phase saturated at a constant CO_2 concentration. The studies have examined the dynamics in only the liquid phase because the solubility of water or hydrocarbons in CO_2 is assumed to be small compared to the CO_2 solubility in the liquid phase. Evaporation of liquid is neglected. These are good approximations at relatively low temperatures and high pressures. Other assumptions may not be as valid. For instance, the liquid phase is treated as being incompressible, and the change in its volume due to CO_2 dissolution is neglected so that the interface remains fixed in position. Compressibility relates to a non-zero divergence of the velocity field. The maximum possible volume change, which is known as swelling, corresponds to when the liquid phase is saturated with CO_2 at the equilibrium concentration. Swelling may be quite significant under relevant conditions of temperatures between 30 and 200 °C and pressures up to 200 bars. The solubility of CO_2 in water can be as high as 8 mass percent under these conditions,[33] and swelling can be as much as 7%. Under the same conditions, the solubility of CO_2 in hydrocarbons can be as high as 50 mass percent, and swelling can be as much as 60%.[2]

In this paper, we perform linear stability analyses to examine the effect of fluid compressibility and interface movement on the onset of buoyancy-driven convection. Previous stability analyses

have neglected the former, while the effect of interface movement has been examined only recently by Meulenbroek *et al.*[34] We address fluid compressibility in Sec. II. We analyze how the non-zero divergence affects the critical time and critical wavenumber. We use thermodynamics to derive expressions for the two physical processes that contribute to the divergence. This allows us to achieve two purposes: (1) gain insight into our results regarding compressibility, and (2) demonstrate the link between compressibility and the volume change from CO_2 dissolution, i.e., the moving interface. Section III presents a stability analysis with the moving interface. We compare our results to those obtained by Meulenbroek *et al.*[34] Our work is applicable to both CO_2 improved oil recovery and CO_2 sequestration, but for clarity and for reasons mentioned later, we focus mainly on the latter. In the appropriate sections, we discuss how compressibility and interface movement may be more pronounced in hydrocarbons than in water. We conclude with a summary of our main results in Sec. IV.

II. FLUID COMPRESSIBILITY

A. Governing and constitutive equations

Our system is an isothermal binary mixture of CO_2 and water (or a liquid hydrocarbon) residing in an inert, permeable, rectangular medium of height H that is homogeneous and isotropic in its porosity ϕ and permeability k. The z axis is centered at the interface, which forms the top boundary, and points upward so that porous domain is defined between $z = -H$ at the bottom and $z = 0$ at the interface. The viscosity μ and diffusion coefficient D are constants. The diffusive flux is given by Fick's law as $\boldsymbol{J} = -\phi\rho D\nabla c$, where ρ is the mass density and c is the CO_2 mass fraction. Fluid flow is governed by Darcy's law which relates the velocity field $\boldsymbol{q} = (u, v, w)^T$ to the pressure gradient ∇p and the gravitational force $-\rho g\nabla z$. We also have the continuity equation and a CO_2 species balance. These equations may be expressed, respectively, as

$$\boldsymbol{q} = -\frac{k}{\mu}\left(\nabla p + \rho g\nabla z\right), \tag{1}$$

$$\phi\frac{\partial\rho}{\partial t} + \nabla\cdot(\rho\boldsymbol{q}) = 0, \tag{2}$$

$$\phi\frac{\partial c\rho}{\partial t} = -\nabla\cdot(c\rho\boldsymbol{q}) + \phi D\nabla\cdot(\rho\nabla c). \tag{3}$$

Substituting (2) into (3), we obtain

$$\left(\phi\frac{\partial}{\partial t} + \boldsymbol{q}\cdot\nabla\right)c = \frac{\mathrm{d}c}{\mathrm{d}t} = \phi D\left(\frac{1}{\rho}\nabla\rho\cdot\nabla c + \nabla^2 c\right), \tag{4}$$

where $\mathrm{d}/\mathrm{d}t = \phi\partial/\partial t + \boldsymbol{q}\cdot\nabla$ denotes the total time derivative (or material derivative) operator. The density obeys the constitutive equation used in previous studies

$$\rho = \rho_0(1 + \alpha c). \tag{5}$$

We have previously shown[24] that (5) is a Taylor series approximation about $c = 0$ at a particular pressure p. Its validity depends on the specific fluid mixture and the conditions considered. The equation is accurate for CO_2-water mixtures under the conditions mentioned in Sec. I. The density of pure water (or hydrocarbon) is ρ_0. We show in Sec. II D that ρ_0 and α depend on temperature, but are nearly invariant with respect to pressure and composition so that they may be approximated as being constants in our isothermal system. As a result, (5) is linear in c. Using (5) and letting $P = p + \rho_0 gz$, (1) becomes

$$\boldsymbol{q} = -\frac{k}{\mu}\left(\nabla P + \rho_0\alpha cg\nabla z\right). \tag{6}$$

The liquid side of the interface is saturated with CO_2 at a fixed mass fraction c_{sat}. Initially, CO_2 is present only at the interface, and the bulk is pure water (or hydrocarbon). The maximum increase in

density from CO_2 dissolution is $\Delta\rho = \rho_0 \alpha c_{sat}$. It is less than 2% of ρ_0 for CO_2-water mixtures, but it can be as high as several percent of ρ_0 for CO_2-hydrocarbons.[35] Rearranging (2) gives

$$\nabla \cdot \boldsymbol{q} = -\frac{1}{\rho}\frac{\mathrm{d}\rho}{\mathrm{d}t}. \tag{7}$$

Since $\rho = \rho(T, p, c)$, the temperature T is a constant, and $\partial\rho/\partial p \approx 0$, we have

$$\nabla \cdot \boldsymbol{q} = -\frac{1}{\rho}\frac{\partial\rho}{\partial c}\frac{\mathrm{d}c}{\mathrm{d}t} = -\frac{\rho_0\alpha}{\rho}\frac{\mathrm{d}c}{\mathrm{d}t}.$$

Substituting (4), we get

$$\nabla \cdot \boldsymbol{q} = -\frac{\phi D \rho_0 \alpha}{\rho}\left(\frac{1}{\rho}\nabla\rho \cdot \nabla c + \nabla^2 c\right). \tag{8}$$

Equation (8) shows that the divergence of $\boldsymbol{q}$ at a point in space is proportional to the divergence of the diffusive flux at that point. We follow earlier works[13,16,26] and nondimensionalize our equations with a velocity scale $\mho = k\Delta\rho g/\mu$, a length scale $\ell = (\phi D)/\mho = (D\phi\mu)/(k\Delta\rho g)$, and a time scale $\tau = (\phi\ell)/\mho = D\,[(\phi\mu)/(k\Delta\rho g)]^2$. We define the dimensionless variables

$$(\tilde{x}, \tilde{y}, \tilde{z})^T = \frac{1}{\ell}(x, y, z)^T,$$

$$\tilde{\boldsymbol{q}} = (\tilde{u}, \tilde{v}, \tilde{w})^T = \frac{1}{\mho}(u, v, w)^T,$$

$$\tilde{t} = \frac{1}{\tau}t, \quad \tilde{c} = \frac{1}{c_{sat}}c, \quad \tilde{P} = \frac{1}{\Delta\rho g \ell}P.$$

In nondimensional terms, the quantity in parentheses on the right hand side of (4) or (8) is $(c_{sat}/\ell^2)[(\Delta\rho/\rho)|\nabla\tilde{c}|^2 + \nabla^2\tilde{c}]$. The $(\Delta\rho/\rho)|\nabla\tilde{c}|^2$ term is negligible compared to $\nabla^2\tilde{c}$ because $|\nabla\tilde{c}|^2 = \nabla\tilde{c}\cdot\nabla\tilde{c}$ is on the same order as $\nabla^2\tilde{c}$, but $\Delta\rho \ll \rho$. We use this approximation and nondimensionalize (4), (6), and (8) to get

$$\frac{\partial\tilde{c}}{\partial t} = -\tilde{\boldsymbol{q}}\cdot\nabla\tilde{c} + \nabla^2\tilde{c}, \tag{9}$$

$$\tilde{\boldsymbol{q}} = -\nabla\tilde{P} - \tilde{c}\nabla\tilde{z}, \tag{10}$$

$$\nabla\cdot\tilde{\boldsymbol{q}} = -\frac{\Delta\rho}{\rho}\nabla^2\tilde{c}. \tag{11}$$

In this choice of scaling, the Rayleigh number $\mathrm{Ra} = H/\ell = (k\Delta\rho g H)/(\phi\mu D)$ does not appear in the governing equations. Instead, Ra appears in the location of the bottom boundary so that porous domain is defined in the range $-\mathrm{Ra} \le \tilde{z} \le 0$. At the onset of convection, the CO_2 concentration will be small at the bottom boundary for sufficiently tall domains. This implies that the bottom boundary becomes irrelevant for large enough values of H. Slim and Ramakrishan[16] have shown that the results of the stability analysis are independent of the Rayleigh number for domains where $\mathrm{Ra} > 75$.

B. The base state

The base state is characterized by a pressure field $\tilde{P}_{base}$ and the absence of bulk fluid motion ($\tilde{\boldsymbol{q}}_{base} = \boldsymbol{0}$). The CO_2 concentration profile $\tilde{c}_{base}(\tilde{z}, \tilde{t})$ of the base state obeys

$$\frac{\partial\tilde{c}_{base}}{\partial\tilde{t}} = \frac{\partial^2\tilde{c}_{base}}{\partial\tilde{z}^2}. \tag{12}$$

We stated in Sec. II A that the bottom boundary of the porous domain is irrelevant for our problem. To simplify the calculations, we treat the domain as a semi-infinite medium where $-\infty < \tilde{z} \le 0$.

The initial/boundary conditions are

$$\tilde{c}_{\text{base}}(\tilde{z}, \tilde{t} = 0) = 0, \quad -\infty < \tilde{z} < 0, \tag{13}$$

$$\tilde{c}_{\text{base}}(\tilde{z} \to -\infty, \tilde{t}) = 0, \quad \forall \tilde{t}, \tag{14}$$

$$\tilde{c}_{\text{base}}(\tilde{z} = 0, \tilde{t}) = 1, \quad \forall \tilde{t}. \tag{15}$$

The solution to (12) with the initial/boundary conditions (13)–(15) is

$$\tilde{c}_{\text{base}}(\tilde{z}, \tilde{t}) = 1 + \text{erf}(\tilde{z}/2\sqrt{\tilde{t}}), \tag{16}$$

where erf(x) is the error function.[16] Applying Leibniz's rule to (16) yields

$$\frac{\partial \tilde{c}_{\text{base}}}{\partial \tilde{z}} = \frac{2}{\sqrt{\pi}} \exp\left(\frac{-\tilde{z}^2}{4\tilde{t}}\right) \frac{\partial}{\partial \tilde{z}} \left(\frac{\tilde{z}}{2\sqrt{\tilde{t}}}\right) = \frac{1}{\sqrt{\pi \tilde{t}}} \exp\left(\frac{-\tilde{z}^2}{4\tilde{t}}\right), \tag{17}$$

$$\frac{\partial^2 \tilde{c}_{\text{base}}}{\partial \tilde{z}^2} = -\frac{\tilde{z}}{2(\pi \tilde{t}^3)^{1/2}} \exp\left(\frac{-\tilde{z}^2}{4\tilde{t}}\right). \tag{18}$$

C. Linearized perturbation equations

1. Formulation

The perturbations to the base state are defined as

$$\tilde{\boldsymbol{q}}' = \tilde{\boldsymbol{q}} = \left(\tilde{u}', \tilde{v}', \tilde{w}'\right)^T, \tag{19}$$

$$\tilde{P}' = \tilde{P} - \tilde{P}_{\text{base}}, \tag{20}$$

$$\tilde{c}' = \tilde{c} - \tilde{c}_{\text{base}}. \tag{21}$$

We substitute (19)–(21) into (9)–(11) and linearize the equations (neglect products of perturbations) to obtain

$$\frac{\partial \tilde{c}'}{\partial \tilde{t}} = -\tilde{w}' \frac{\partial \tilde{c}_{\text{base}}}{\partial \tilde{z}} + \nabla^2 \tilde{c}', \tag{22}$$

$$\tilde{\boldsymbol{q}}' = -\nabla \tilde{P}' - \tilde{c}' \nabla \tilde{z}, \tag{23}$$

$$\nabla \cdot \tilde{\boldsymbol{q}}' = -\frac{\Delta\rho}{\rho} \left(\nabla^2 \tilde{c}' + \frac{\partial^2 \tilde{c}_{\text{base}}}{\partial \tilde{z}^2}\right). \tag{24}$$

Following previous work,[11–16] we eliminate $\tilde{P}'$, $\tilde{u}'$, and $\tilde{v}'$ by taking twice the curl of (23), using the identity $\nabla \times \nabla \times \tilde{\boldsymbol{q}}' = \nabla(\nabla \cdot \tilde{\boldsymbol{q}}') - \nabla^2 \tilde{\boldsymbol{q}}'$, applying (24), and equating the vertical components to obtain

$$\nabla^2 \tilde{w}' = -\nabla_{\text{h}}^2 \tilde{c}' - \frac{\partial}{\partial \tilde{z}} \left[\frac{\Delta\rho}{\rho} \left(\nabla^2 \tilde{c}' + \frac{\partial^2 \tilde{c}_{\text{base}}}{\partial \tilde{z}^2}\right)\right], \tag{25}$$

where $\nabla_{\text{h}}^2 = \partial^2/\partial \tilde{x}^2 + \partial^2/\partial \tilde{y}^2$ is the horizontal Laplacian. Using (5) with the quantities $\Delta\rho = \rho_0 \alpha c_{\text{sat}}$ and $\tilde{c} = \tilde{c}_{\text{base}} + \tilde{c}'$ defined in Sec. II A, the second term on the right hand side of (25) is

$$-\frac{\partial}{\partial \tilde{z}} \left[\frac{\Delta\rho}{\rho} \left(\nabla^2 \tilde{c}' + \frac{\partial^2 \tilde{c}_{\text{base}}}{\partial \tilde{z}^2}\right)\right] = -\frac{1}{[1/(\alpha c_{\text{sat}}) + \tilde{c}]} \left(\frac{\partial}{\partial \tilde{z}} \nabla^2 \tilde{c}' + \frac{\partial^3 \tilde{c}_{\text{base}}}{\partial \tilde{z}^3}\right)$$
$$+ \frac{1}{[1/(\alpha c_{\text{sat}}) + \tilde{c}]^2} \left(\nabla^2 \tilde{c}' + \frac{\partial^2 \tilde{c}_{\text{base}}}{\partial \tilde{z}^2}\right) \left(\frac{\partial \tilde{c}'}{\partial \tilde{z}} + \frac{\partial \tilde{c}_{\text{base}}}{\partial \tilde{z}}\right).$$

The nondimensionalized mass fraction $\tilde{c}$ is less than or equal to one. We show in Sec. II D that over the range of conditions stated in Sec. I, α varies between 0.27 and 0.30 for CO_2-water mixtures. The interfacial mass fraction c_{sat} may be as large as 0.08 for CO_2-water. Thus, $1/(\alpha c_{sat})$ is typically one or two orders of magnitude larger than $\tilde{c}$. We may neglect $\tilde{c}$ when it is added to $1/(\alpha c_{sat})$ and linearize (25) to get

$$\nabla^2\tilde{w}' = -\nabla_h^2\tilde{c}' - \alpha c_{sat}\left(\frac{\partial}{\partial\tilde{z}}\nabla^2\tilde{c}' + \frac{\partial^3\tilde{c}_{base}}{\partial\tilde{z}^3}\right) + (\alpha c_{sat})^2\left[\left(\nabla^2\tilde{c}'\right)\frac{\partial\tilde{c}_{base}}{\partial\tilde{z}} + \frac{\partial\tilde{c}'}{\partial\tilde{z}}\frac{\partial^2\tilde{c}_{base}}{\partial\tilde{z}^2} + \frac{\partial\tilde{c}_{base}}{\partial\tilde{z}}\frac{\partial^2\tilde{c}_{base}}{\partial\tilde{z}^2}\right].$$

Terms involving only $c_{base}(\tilde{z},\tilde{t})$ vanish if we apply the horizontal Laplacian to both sides

$$\nabla^2\left(\nabla_h^2\tilde{w}'\right) = -\nabla_h^2\left(\nabla_h^2\tilde{c}'\right) - \alpha c_{sat}\frac{\partial}{\partial\tilde{z}}\nabla^2\left(\nabla_h^2\tilde{c}'\right) + (\alpha c_{sat})^2\left\{\left[\nabla^2\left(\nabla_h^2\tilde{c}'\right)\right]\frac{\partial\tilde{c}_{base}}{\partial\tilde{z}} + \left[\frac{\partial}{\partial\tilde{z}}\left(\nabla_h^2\tilde{c}'\right)\right]\frac{\partial^2\tilde{c}_{base}}{\partial\tilde{z}^2}\right\}. \quad (26)$$

The medium is taken to be infinitely large in $\tilde{x}$ and $\tilde{y}$ so that we may neglect interactions with the lateral boundaries and allow for perturbations of arbitrary wavenumbers. Differentiation in these horizontal directions may be simplified by expressing the perturbations $\tilde{c}'$ and $\tilde{w}'$ in terms of the Fourier transforms $\hat{c}'(\tilde{s},\tilde{z},\tilde{t})$ and $\hat{w}'(\tilde{s},\tilde{z},\tilde{t})$, where $\tilde{s}$ is a dimensionless wavenumber. This wavenumber is defined as $\tilde{s} = \sqrt{\tilde{s}_x^2 + \tilde{s}_y^2}$, where $\tilde{s}_x$ and $\tilde{s}_y$ are the dimensionless wavenumbers in $\tilde{x}$ and $\tilde{y}$, respectively. The Fourier transforms give a clear physical interpretation of the perturbations. Each mode may be thought of as a wave in the $\tilde{x}\tilde{y}$ plane specified by a wavenumber $\tilde{s}$. Perturbations are represented as linear superpositions over all possible modes, with $\hat{c}'$ and $\hat{w}'$ (which may be interpreted as wave amplitudes) acting as weighting factors. Equations (22) and (26) in terms of the Fourier transforms are

$$\frac{\partial\hat{c}'}{\partial\tilde{t}} = -\hat{w}'\frac{\partial\tilde{c}_{base}}{\partial\tilde{z}} + \left(\frac{\partial^2}{\partial\tilde{z}^2} - \tilde{s}^2\right)\hat{c}', \quad (27)$$

$$\left(\frac{\partial^2}{\partial\tilde{z}^2} - \tilde{s}^2\right)\hat{w}' = \tilde{s}^2\hat{c}' - \alpha c_{sat}\left(\frac{\partial^2}{\partial\tilde{z}^2} - \tilde{s}^2\right)\frac{\partial\hat{c}'}{\partial\tilde{z}} + (\alpha c_{sat})^2\left\{\left[\left(\frac{\partial^2}{\partial\tilde{z}^2} - \tilde{s}^2\right)\hat{c}'\right]\frac{\partial\tilde{c}_{base}}{\partial\tilde{z}} + \frac{\partial\hat{c}'}{\partial\tilde{z}}\frac{\partial^2\tilde{c}_{base}}{\partial\tilde{z}^2}\right\}. \quad (28)$$

For an incompressible fluid, only the first term on the right hand side of (28) appears. The terms which depend on α and $\tilde{c}_{sat}$ arise from the non-zero divergence of $\tilde{\boldsymbol{q}}'$. Equations (27) and (28) form a set of coupled partial differential equations for $\hat{c}'(\tilde{s},\tilde{z},\tilde{t})$ and $\hat{w}'(\tilde{s},\tilde{z},\tilde{t})$. The boundary conditions are

$$\hat{w}'(\tilde{s},\tilde{z}\to-\infty,\tilde{t}) = \hat{c}'(\tilde{s},\tilde{z}\to-\infty,\tilde{t}) = 0, \quad \forall\tilde{s},\tilde{t}, \quad (29)$$

$$\hat{w}'(\tilde{s},\tilde{z}=0,\tilde{t}) = \hat{c}'(\tilde{s},\tilde{z}=0,\tilde{t}) = 0, \quad \forall\tilde{s},\tilde{t}. \quad (30)$$

The boundary condition $\hat{c}'(\tilde{s},\tilde{z}=0,\tilde{t}) = 0$ follows from the fact that at the interface, we have $\tilde{c} = \tilde{c}_{base} + \tilde{c}' = 1$ and $\tilde{c}_{base} = 1$ so that $\tilde{c}'$ must be zero. The boundary condition $\hat{w}'(\tilde{s},\tilde{z}=0,\tilde{t}) = 0$ for the liquid vertical velocity through the interface is also used in previous stability analyses.[11–16] This velocity may be approximated as zero because evaporation of liquid is neglected, as we stated in Sec. I.

2. Non-modal stability analysis

In summary, the stability analysis solves (27) and (28) for $\hat{c}'$ and $\hat{w}'$, with boundary conditions (29) and (30) and $\tilde{c}_{base}$ given by (16). We solve these equations with the non-modal stability analysis

described earlier.[15,19] The Laplacian operator L and its inverse L^{-1} in Fourier space are

$$\mathrm{L} = \frac{\partial^2}{\partial \tilde{z}^2} - \tilde{s}^2, \tag{31}$$

$$\mathrm{L}^{-1} = \left(\frac{\partial^2}{\partial \tilde{z}^2} - \tilde{s}^2 \right)^{-1}, \tag{32}$$

respectively. In the non-modal stability analysis, we combine (27) and (28) to get

$$\frac{\partial \hat{c}'}{\partial \tilde{t}} = \left\{ -\frac{\partial \tilde{c}_{\mathrm{base}}}{\partial \tilde{z}} \left[\tilde{s}^2 \mathrm{L}^{-1} - \alpha c_{\mathrm{sat}} \frac{\partial}{\partial \tilde{z}} + (\alpha c_{\mathrm{sat}})^2 \left(\frac{\partial \tilde{c}_{\mathrm{base}}}{\partial \tilde{z}} + \frac{\partial^2 \tilde{c}_{\mathrm{base}}}{\partial \tilde{z}^2} \mathrm{L}^{-1} \frac{\partial}{\partial \tilde{z}} \right) \right] + \mathrm{L} \right\} \hat{c}', \tag{33}$$

where the base state derivatives are given by (17) and (18). We numerically integrate (33) over time by discretizing $\hat{c}'$ in $\tilde{z}$ using finite differences on a uniformly spaced mesh with N grid points spaced apart by a distance $\Delta\tilde{z}$

$$\tilde{z}_i = -(i-1)\Delta\tilde{z}, \quad i = 1, 2, \ldots, N, \tag{34}$$

$$\boldsymbol{c}(\tilde{s}, \tilde{t}) = \hat{c}'(\tilde{s}, \tilde{z}_i, \tilde{t}), \quad i = 1, 2, \ldots, N. \tag{35}$$

Following Bestehorn and Firoozabadi,[19] we achieve a high spatial resolution by considering only the top 10% of a large, but finite domain defined in the range $-\mathrm{Ra}/10 \le \tilde{z} \le 0$. The value of the Rayleigh number Ra is chosen to be sufficiently large so that the system does not feel the effect of the bottom boundary. We use $\mathrm{Ra} = 1600$ and $N = 256$ so that $\Delta\tilde{z} = 160/255 = 32/51$. The discretization in $\tilde{z}$ transforms (33) to

$$\frac{\mathrm{d}\boldsymbol{c}}{\mathrm{d}\tilde{t}} = \mathbf{M}\boldsymbol{c}, \tag{36}$$

where $\mathbf{M}$ is a $N \times N$ matrix that represents the operator acting on $\hat{c}'$ in (33). The wavenumber $\tilde{s}$ enters (36) as a parameter. A few studies[11,12,14] numerically integrate a matrix equation that is analogous to (36) by using a "white noise" initial condition where the amplitude $\hat{c}'$ of all perturbation modes are equal to unity at $\tilde{t} = 0$. This condition leads to the earliest critical time compared to some other initial conditions for a related problem in free space (cavities without porous media).[36] However, the white noise condition does not necessarily lead to the earliest critical time in our problem.[15,16] The underlying issue is that it is not clear what the most physically realistic initial condition for $\boldsymbol{c}$ should be. The non-modal stability analysis circumvents this problem by defining a $N \times N$ propagator matrix $\mathbf{P}(\tilde{s}, \tilde{t})$ that relates the vector $\boldsymbol{c}(\tilde{s}, \tilde{t} = 0)$ at the initial time to its value $\boldsymbol{c}(\tilde{s}, \tilde{t})$ at a later time

$$\boldsymbol{c}(\tilde{s}, \tilde{t}) = \mathbf{P}\boldsymbol{c}(\tilde{s}, \tilde{t} = 0). \tag{37}$$

Substitution of (37) into (36) leads to

$$\frac{\mathrm{d}\mathbf{P}}{\mathrm{d}\tilde{t}} = \mathbf{M}\mathbf{P}. \tag{38}$$

We integrate (38) instead of (36) to update the propagator matrix over time. It is clear from (37) that $\mathbf{P}$ should initially be equal to the identity matrix. We use the fourth-order Runge-Kutta method to integrate (38) over time $\tilde{t}$ for many values of the wavenumber $\tilde{s}$. The integration begins at an initial time of $\tilde{t} = 0.01$; the singularity at $\tilde{t} = 0$ of (17) and (18) prohibits starting the integration at very early times. The integration ends at $\tilde{t} = 300$, and the step size is $\Delta\tilde{t} \approx 300/2000 = 3/20$. We have checked our results for convergence with respect to the values of N, $\Delta\tilde{z}$, $\Delta\tilde{t}$, and the initial time.

Before the onset of convection, all perturbation modes decay with time because they are dissipated by diffusion. We define the critical time $\tilde{t}_{\mathrm{c}}$ to be the earliest instance (the minimum time over all wavenumbers) when a perturbation mode begins to grow. The instantaneous growth rate at time $\tilde{t}$ of a mode with wavenumber $\tilde{s}$ is

$$\varsigma = \frac{1}{\varrho} \frac{\mathrm{d}\varrho}{\mathrm{d}\tilde{t}}, \tag{39}$$

where $\varrho = \varrho(\tilde{s}, \tilde{t})$ is the spectral radius of $\mathbf{P}$. The critical time may be defined as the first instance when $\varsigma > 0$. The wavenumber that corresponds to the critical time is the critical wavenumber $\tilde{s}_c$. We consider wavenumbers between $10^{-4} \leq \tilde{s} \leq 0.15$ and times between $0.01 \leq \tilde{t} \leq 300$, and we divide these intervals into 400 and 2000 evenly spaced points, respectively. Essentially, we compute ς at each of the 400×2000 points in wavenumber–time space by integrating (38) over time for each value of the wavenumber and calculating $\varsigma(\tilde{s}, \tilde{t})$.

D. Results and discussion

We see from (28) that the terms which arise from the non-zero divergence depend on both α and c_{sat}. Our previous work[24] has studied a CO_2-water mixture where the temperature is 30 °C, and the pressure at the interface is 50 bars. We have used the cubic-plus-association (CPA) equation of state[33] to find that $\alpha = 0.27$ and $c_{sat} = 0.043$ at this temperature and pressure. Figure 1 depicts the marginal stability ($\varsigma = 0$) contours in wavenumber–time space for these values of α and c_{sat}. The base state is unstable above the contours, where $\varsigma > 0$ and the onset of convection has occurred. It is stable below the contours. Figure 1 shows that the effect of compressibility is negligible, as there is nearly complete overlap between the two contours. The critical time $\tilde{t}_c$ and the critical wavenumber $\tilde{s}_c$ are given by the minimum of the corresponding contours. We have $\tilde{t}_c \approx 50.4$ and $\tilde{s}_c \approx 0.0666$ for a compressible fluid. For an incompressible fluid, we have a slightly earlier critical time of $\tilde{t}_c \approx 50.2$, which agrees with the result from Bestehorn and Firoozabadi.[19]

Our study considers temperatures between 30 and 200 °C and pressures up to 200 bars, as stated in Sec. I. We expect fluid compressibility to have a negligible effect on the critical time and the critical wavenumber in CO_2-water mixtures under these conditions. We justify this assertion by examining the range of values for α and c_{sat}. Table I presents values for relevant parameters. We have previously shown[24] that

$$\alpha = 1 - \rho_0 \left(\frac{\bar{V}_1 + c_1}{M_1} \right). \tag{40}$$

The density ρ_0 decreases from about 1000 kg/m^3 at 30 °C to about 870 kg/m^3 at 200 °C and has a relatively weak dependence on pressure (see, e.g., the NIST Chemistry WebBook). Water at 200 °C is a gas for pressures below 15.5 bars. We have used the CPA equation of state[33] to find that the partial molar volumes $\bar{V}_1$ and $\bar{V}_2$ depend on temperature, but are nearly constant with respect to pressure and composition (variation is less than 1%). The CO_2 shift parameter c_1 is a constant, while the H_2O shift parameter c_2 is a function of temperature only[33] and is small compared to $\bar{V}_2$. Thus,

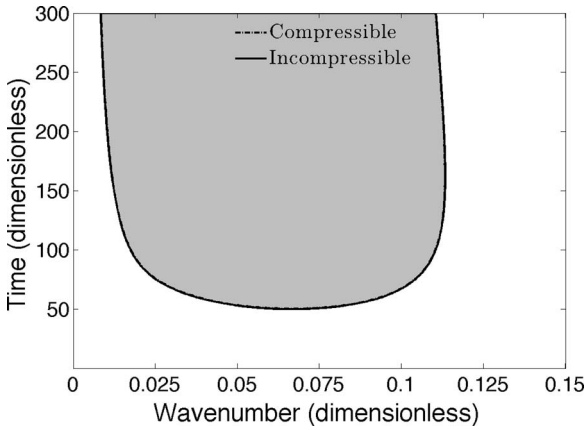

FIG. 1. Marginal stability ($\varsigma = 0$) contours in wavenumber–time space. The base state is unstable in the shaded region above the contours, where $\varsigma > 0$ and the onset of convection has occurred. It is stable below the contours. The dashed-dotted contour lies slightly above the solid contour, but there is nearly complete overlap. This indicates that fluid compressibility does not significantly affect the critical time $\tilde{t}_c$ or the critical wavenumber $\tilde{s}_c$.

TABLE I. Parameter values for temperatures between 30 and 200 °C and pressures up to 200 bars.

Symbol	Definition	Range of values
ρ_0	Density of pure water	1004 kg/m^3 (200 bars)–995 kg/m^3 (1 bar) at 30 °C 878 kg/m^3 (200 bars)–864 kg/m^3 (15.5 bars) at 200 °C
$\bar{V}_1$	CO_2 partial molar volume	3.5×10^{-5} m^3/mole (30 °C)–3.9×10^{-5} m^3/mole (200 °C)
c_1	CO_2 shift parameter	-3.1×10^{-6} m^3/mole
M_1	CO_2 molar mass	44×10^{-3} kg/mole
$\bar{V}_2$	H_2O partial molar volume	1.76×10^{-5} m^3/mole (30 °C)–1.86×10^{-5} m^3/mole (200 °C)
c_2	H_2O shift parameter	3.6×10^{-7} m^3/mole (30 °C) to -3.5×10^{-7} m^3/mole (200 °C)
M_2	H_2O molar mass	18×10^{-3} kg/mole
c_{sat}	Maximum CO_2 solubility	Up to 8 mass percent (at 30 °C and 200 bars)

α depends primarily on temperature, and we may approximate it as a constant in our isothermal system. It ranges between 0.27 and 0.30 for CO_2-water mixtures. Since c_{sat} may be as high as 8% for CO_2-water, the product αc_{sat} may be up to twice as large as the value used in our stability analysis. However, it is clear from Figure 1 that fluid compressibility will not significantly affect the onset of convection even for this large value.

We gain insight into why compressibility has a negligible effect in CO_2-water mixtures if we examine the divergence of the velocity field. Equation (7) relates $\nabla \cdot \boldsymbol{q}$ to the total time derivative of the mass density $\rho = m/V$. The mass density of a fluid particle may change if its mass m or its volume V changes so that

$$\nabla \cdot \boldsymbol{q} = \frac{1}{V}\frac{\mathrm{d}V}{\mathrm{d}t} - \frac{1}{m}\frac{\mathrm{d}m}{\mathrm{d}t} = \frac{1}{V}\left(\frac{\mathrm{d}V}{\mathrm{d}t} - \frac{1}{\rho}\frac{\mathrm{d}m}{\mathrm{d}t}\right). \tag{41}$$

There are two contributions to the compressibility: (1) a change in the volume, which is expressed by the first term in the parentheses, and (2) a change in the mass, which is expressed by the second term in the parentheses. We may estimate the relative importance of the two contributions as follows. From thermodynamics,[37] we have

$$V = (\bar{V}_1 + c_1)n_1 + (\bar{V}_2 + c_2)n_2, \tag{42}$$

where n_1 and n_2 represent the moles of CO_2 and water, respectively, in the fluid particle. Since the partial molar volumes may be approximated as constants, we have

$$\mathrm{d}V = (\bar{V}_1 + c_1)\mathrm{d}n_1 + (\bar{V}_2 + c_2)\mathrm{d}n_2,$$

$$\mathrm{d}m = M_1\mathrm{d}n_1 + M_2\mathrm{d}n_2.$$

Using values of $\bar{V}_1 + c_1 = 3.2 \times 10^{-5}$ m^3/mole, $\bar{V}_2 + c_2 = 1.8 \times 10^{-5}$ m^3/mole, and $\rho = 1000$ kg/m^3, we find

$$\frac{\mathrm{d}V}{\mathrm{d}t} = (3.2 \times 10^{-5})\frac{\mathrm{d}n_1}{\mathrm{d}t} + (1.8 \times 10^{-5})\frac{\mathrm{d}n_2}{\mathrm{d}t}, \tag{43}$$

$$\frac{1}{\rho}\frac{\mathrm{d}m}{\mathrm{d}t} = (4.4 \times 10^{-5})\frac{\mathrm{d}n_1}{\mathrm{d}t} + (1.8 \times 10^{-5})\frac{\mathrm{d}n_2}{\mathrm{d}t}. \tag{44}$$

From (43) and (44), we see that $\mathrm{d}V/\mathrm{d}t$ can be similar in magnitude to $(1/\rho)\mathrm{d}m/\mathrm{d}t$. In other words, the volume change term in (41) is comparable to the mass change term so that they largely cancel each other to produce a relatively small divergence. This shows why the non-zero $\nabla \cdot \boldsymbol{q}$ has a negligible effect on the onset of convection in CO_2-water mixtures. Volume change causes movement of the interface. We investigate the consequences of a moving interface on the onset of convection in Sec. III.

We conclude this section with a discussion of two key points. First, we note that compressibility is likely to be more significant in CO_2-hydrocarbon mixtures due to the higher CO_2 solubility in

hydrocarbons (see Sec. I). However, the linear density equation of state (5) is expected to be invalid for very high solubility hydrocarbons since c is required to be sufficiently small, and we cannot perform a linear stability analysis for such mixtures. Another complication is that CO_2 dissolution may significantly change the viscosity[2,3] and the partial molar volumes[37] of the hydrocarbon phase, so that μ and α cannot be approximated as constants. The second key point is that compressibility may be important for CO_2 sequestration even if it does not noticeably affect the onset of convection in the aqueous phase. Numerical simulations have shown that both rock compressibility and fluid compressibility can significantly reduce the pressure buildup that occurs during CO_2 injection.[38] As we mentioned in Sec. I, the pressure reduction has implications for the long-term storage security of CO_2 in saline aquifers. It may lower the risk of cap rock fracture and subsequent CO_2 leakage back into the atmosphere.

III. INTERFACE MOVEMENT

A. Governing and constitutive equations

Much of our formulation in Sec. III remains the same as in Sec. II. There are two important differences, however: (1) we treat the liquid (aqueous or hydrocarbon) phase as being incompressible ($\nabla \cdot \boldsymbol{q} = 0$), and (2) the position $h(t)$ of the interface between the CO_2 phase and the liquid phase moves with time as a result of the volume change from CO_2 dissolution. We consider a semi-infinite medium where $-\infty < z \le h(t)$, with $h(0) = 0$. The velocity $\mathrm{d}h/\mathrm{d}t$ with which the interface moves can be obtained from performing mass balances across the interface. The total mass balance and CO_2 mass balance across the interface are,[39–41] respectively,

$$\phi\rho^G\left(w_{\mathrm{t}}^G - \frac{\mathrm{d}h}{\mathrm{d}t}\right) = \phi\rho^L\left(w_{\mathrm{t}}^L - \frac{\mathrm{d}h}{\mathrm{d}t}\right), \tag{45}$$

$$-\phi\rho^G D^G\frac{\partial c^G}{\partial z} + \phi c^G\rho^G\left(w_{\mathrm{t}}^G - \frac{\mathrm{d}h}{\mathrm{d}t}\right) = -\phi\rho^L D^L\frac{\partial c^L}{\partial z} + \phi c^L\rho^L\left(w_{\mathrm{t}}^L - \frac{\mathrm{d}h}{\mathrm{d}t}\right), \tag{46}$$

where G denotes the CO_2-rich side of the interface, L denotes the liquid side of the interface, and w_{t} is the true vertical velocity. This velocity is related to the Darcy vertical velocity w by $w_{\mathrm{t}} = w/\phi$. The composition derivatives $\partial c^G/\partial z$ and $\partial c^L/\partial z$ are evaluated at the interface. We combine (45) and (46) to eliminate w_{t}^G and obtain

$$w_{\mathrm{t}}^L - \frac{\mathrm{d}h}{\mathrm{d}t} = -\frac{1}{\left(c^G - c^L\right)}\left(D^L\frac{\partial c^L}{\partial z} - \frac{\rho^G}{\rho^L}D^G\frac{\partial c^G}{\partial z}\right).$$

If we use the fact that $c^G \approx 1$ throughout the entire CO_2 phase because the solubility of liquid in CO_2 is negligible (see Sec. I), the second term in the parentheses vanishes so that

$$\frac{\mathrm{d}h}{\mathrm{d}t} = w_{\mathrm{t}}^L + \frac{D^L}{\left(1 - c^L\right)}\frac{\partial c^L}{\partial z}. \tag{47}$$

We approximate the convective velocity w_{t}^L as being zero because evaporation of liquid is negligible, as stated in Secs. I and II C. Thus, (47) becomes

$$\frac{\mathrm{d}h}{\mathrm{d}t} = \frac{D^L}{\left(1 - c^L\right)}\frac{\partial c^L}{\partial z} = \frac{D}{(1 - c_{\mathrm{sat}})}\left.\frac{\partial c}{\partial z}\right|_{z=h}. \tag{48}$$

The governing equations in nondimensionalized form are given by (9), (10), and

$$\nabla \cdot \tilde{\boldsymbol{q}} = 0, \tag{49}$$

$$\frac{\mathrm{d}\tilde{h}}{\mathrm{d}\tilde{t}} = \frac{c_{\mathrm{sat}}}{(1 - c_{\mathrm{sat}})}\left.\frac{\partial \tilde{c}}{\partial \tilde{z}}\right|_{\tilde{z}=\tilde{h}}, \tag{50}$$

where $\tilde{h} = h/\ell$. The boundary conditions in $\tilde{z}$ are

$$\tilde{c}(\tilde{x}, \tilde{y}, \tilde{z} = \tilde{h}, \tilde{t}) = 1, \quad \forall \tilde{x}, \tilde{y}, \tilde{t}, \tag{51}$$

$$\tilde{w}(\tilde{x}, \tilde{y}, \tilde{z} = \tilde{h}, \tilde{t}) = 0, \quad \forall \tilde{x}, \tilde{y}, \tilde{t}, \tag{52}$$

$$\tilde{c}(\tilde{x}, \tilde{y}, \tilde{z} \to -\infty, \tilde{t}) = \tilde{w}(\tilde{x}, \tilde{y}, \tilde{z} \to -\infty, \tilde{t}) = 0, \quad \forall \tilde{x}, \tilde{y}, \tilde{t}. \tag{53}$$

B. The base state

The base state concentration profile $\tilde{c}_{\text{base}}(\tilde{z}, \tilde{t})$ with a moving interface satisfies the one-dimensional diffusion equation (12), along with (50), the initial condition (13), the bottom boundary condition (14), and the interface boundary condition

$$\tilde{c}_{\text{base}}(\tilde{z} = \tilde{h}, \tilde{t}) = 1, \quad \forall \tilde{t}. \tag{54}$$

The solution of this set of equations is analogous to the solution of the classical Stefan problem, which involves phase changes (e.g., melting of ice) that occur as a result of one-dimensional heat conduction.[42] The moving interface in the Stefan problem represents the front where the phase change occurs. The position $\tilde{h}(\tilde{t})$ of the interface in our problem indicates the extent of the volume change; its value depends on the amount of CO_2 dissolved in the liquid phase. The average CO_2 concentration grows with the square root of time when the interface is fixed in position and the base state is given by (16), as shown earlier.[24,43,44] As an ansatz, we take $\tilde{h}(\tilde{t})$ to be proportional to the square root of time

$$\tilde{h}(\tilde{t}) = 2\eta\sqrt{\tilde{t}}, \tag{55}$$

where η is a dimensionless constant. The solution to (12)–(14) and (54)–(55) is

$$\tilde{c}_{\text{base}}(\tilde{z}, \tilde{t}) = \frac{1 + \text{erf}(\tilde{z}/2\sqrt{\tilde{t}})}{1 + \text{erf}(\eta)}. \tag{56}$$

The base state derivative with respect to $\tilde{z}$ is

$$\frac{\partial \tilde{c}_{\text{base}}}{\partial \tilde{z}} = \frac{\exp(-\tilde{z}^2/4\tilde{t})}{1 + \text{erf}(\eta)} \frac{1}{\sqrt{\pi \tilde{t}}}. \tag{57}$$

By substituting (55) and (57) into (50), we obtain a nonlinear equation

$$\eta[1 + \text{erf}(\eta)] \exp(\eta^2) = \frac{1}{\sqrt{\pi}} \frac{c_{\text{sat}}}{(1 - c_{\text{sat}})}. \tag{58}$$

For a given interfacial mass fraction c_{sat}, we must first solve (58) for η. This value of η can then be substituted into (55) to compute the interface position, into (56) to determine the concentration field, or into (57) to calculate the diffusive flux. In addition to (56), the base state is described by a pressure field $\tilde{P}_{\text{base}}$ and $\tilde{\boldsymbol{q}}_{\text{base}} = \boldsymbol{0}$.

C. Linearized perturbation equations

We follow the procedure described in Sec. II C and introduce perturbations to the base state, linearize the equations, and expand the perturbations using the Fourier transforms $\hat{c}'(\tilde{s}, \tilde{z}, \tilde{t})$ and $\hat{w}'(\tilde{s}, \tilde{z}, \tilde{t})$ to get

$$\frac{\partial \hat{c}'}{\partial \tilde{t}} = \left\{ -\tilde{s}^2 \left[\frac{\exp(-\tilde{z}^2/4\tilde{t})}{1 + \text{erf}(\eta)} \frac{1}{\sqrt{\pi \tilde{t}}} \right] \text{L}^{-1} + \text{L} \right\} \hat{c}'. \tag{59}$$

We perform the non-modal stability analysis described in Sec. II C 2 to numerically integrate a matrix equation analogous to (38) using the same values of N, $\Delta\tilde{z}$, $\Delta\tilde{t}$, and the initial time. The only

difference is that after every time step, each grid point is moved a distance

$$\frac{\mathrm{d}\tilde{h}}{\mathrm{d}\tilde{t}}\Delta\tilde{t} = \frac{\eta}{\sqrt{\tilde{t}}}\Delta\tilde{t},$$

so that the topmost grid point is always located at $\tilde{z} = \tilde{h}$. As a result, we must add

$$\frac{\mathrm{d}\tilde{h}}{\mathrm{d}\tilde{t}}\frac{\partial}{\partial\tilde{z}} = \frac{\eta}{\sqrt{\tilde{t}}}\frac{\partial}{\partial\tilde{z}}, \tag{60}$$

to the matrix $\mathbf{M}$ to account for the movement of the mesh.

D. Results and discussion

Figure 2 illustrates marginal stability contours of $\varsigma = 0$ in wavenumber–time space. Equation (58) shows that the value of η, and therefore the extent of the volume change, depends on c_{sat}. We present results for three different values of c_{sat}: 0.043, 0.08, and 0.12. The first is the same value used in Sec. II D. The second is the maximum solubility of CO_2 in water at the conditions examined in our study. For comparison, we also present results for $c_{\mathrm{sat}} = 0.12$, which could represent a CO_2-hydrocarbon mixture or a CO_2-water mixture at pressures much higher than those considered in our study.[45,46] In all cases, the effect of interface movement is much more prominent than the effect of fluid compressibility. The contours are shifted downward and to the left with increasing values of c_{sat}, which indicates that interface movement decreases the critical time $\tilde{t}_{\mathrm{c}}$ and the critical wavenumber $\tilde{s}_{\mathrm{c}}$. Another way to quantify the effect of interface movement is to plot $\tilde{t}_{\mathrm{c}}$ and $\tilde{s}_{\mathrm{c}}$ as a function of c_{sat}. This relationship is shown in Figure 3. Interface movement becomes negligible in the limit as $c_{\mathrm{sat}} \to 0$. The critical time and critical wavenumber approach the values of $\tilde{t}_{\mathrm{c}} \approx 50.2$ and $\tilde{s}_{\mathrm{c}} \approx 0.0666$ from Sec. II D in this limit. We obtain the following scaling relations for the dimensionalized critical time t_{c} and critical wavenumber s_{c} from the best-fit lines:

$$t_{\mathrm{c}} = (50.2 - 66.4c_{\mathrm{sat}})\tau = (50.2 - 66.4c_{\mathrm{sat}})\left(\frac{D^{1/2}\phi\mu}{k\Delta\rho g}\right)^2, \tag{61}$$

$$s_{\mathrm{c}} = (0.0666 - 0.0192c_{\mathrm{sat}})/\ell = (0.0666 - 0.0192c_{\mathrm{sat}})\left(\frac{k\Delta\rho g}{D\phi\mu}\right). \tag{62}$$

These relations hold as long as c_{sat} is sufficiently small for (5) to be valid (see our discussion in Sec. II A). We summarize our results in Table II, where "% difference" refers to the absolute percent difference compared to the fixed interface. The decrease in $\tilde{t}_{\mathrm{c}}$ in CO_2-water mixtures can be up to

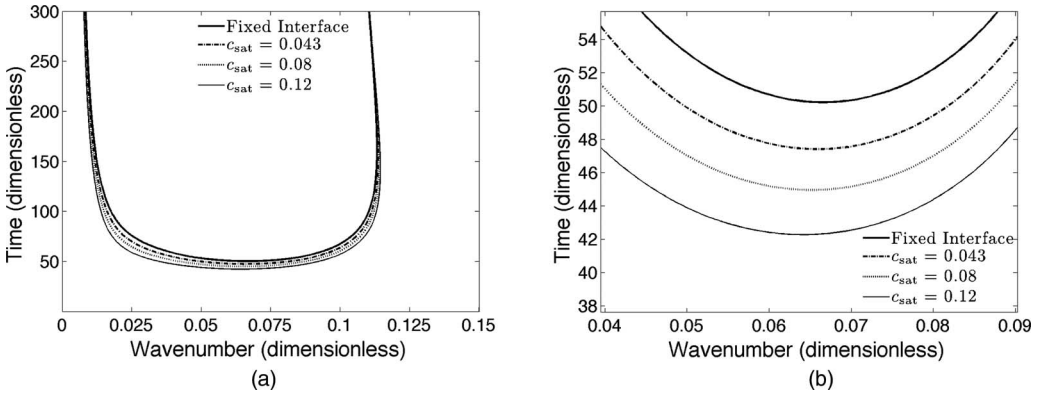

FIG. 2. (a) Marginal stability ($\varsigma = 0$) contours in wavenumber–time space; (b) zoomed-in view around the critical time $\tilde{t}_{\mathrm{c}}$ and the critical wavenumber $\tilde{s}_{\mathrm{c}}$. The moving interface shifts the contours downward and to the left, indicating a decrease in the critical time and critical wavenumber. The effect becomes more pronounced for larger values of the interfacial CO_2 mass fraction c_{sat}.

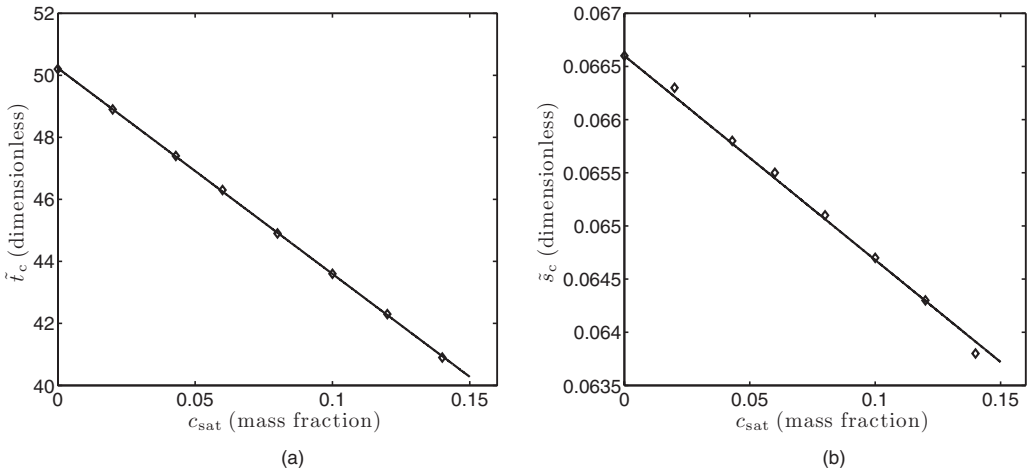

FIG. 3. (a) and (b) The critical time $\tilde{t}_c$ and critical wavenumber $\tilde{s}_c$ for several values of the interfacial CO_2 mass fraction c_{sat}. Interface movement becomes negligible in the limit as $c_{sat} \to 0$. The best-fit lines represent $\tilde{t}_c = 50.2 - 66.4c_{sat}$ and $\tilde{s}_c = 0.0666 - 0.0192c_{sat}$.

around 10% at the conditions examined in our study, but realistically not more than 20% even at very high pressures. In contrast, Meulenbroek *et al.*[34] have found that interface movement can lead to more than a tenfold decrease in $\tilde{t}_c$. They also model the time-dependence of $\tilde{h}$ using (55). However, they determine η not from mass balances, but by examining the volume increase observed in *PVT* cell experiments where CO_2 is mixed with oil or water.[47] Determining η in this way may severely overestimate its magnitude because (55) is valid only before the onset of convection, yet the onset is virtually instantaneous in these experiments so that much of the volume increase is due to the enhanced dissolution by convection. As a result, Meulenbroek *et al.*[34] obtain a range for η between 2 and 4, values that are roughly 100 times larger than our values. We expect the effect of interface movement to be much less pronounced than predicted by their analysis.

Nevertheless, since the time scale τ varies inversely with the square of the permeability k, a 10% reduction in $\tilde{t}_c$ can still be significant in low permeability media where τ is large. For a representative set of conditions where $D = 2 \times 10^{-9}$ m^2/s, $\phi = 0.2$, $\mu = 0.001$ Pa s, $k = 0.1$ darcy, and $\Delta\rho = 10$ kg/m^3, we have $\tau \approx 10$ days. A 10% reduction in $\tilde{t}_c$ is equivalent to a decrease in the critical time t_c of about 50 days for these conditions. If instead $k = 0.01$ darcy (it is not uncommon to find such low permeability formations), a 10% reduction in $\tilde{t}_c$ corresponds to a time period of about 5000 days $\approx$ 13.5 years.

Movement of the interface affects the critical time in two opposing ways. Comparing (16) and (56), we see that the ratio of the concentration field $\tilde{c}_{base}$ when the interface moves with

TABLE II. Summary of results in Figure 3. Interface movement may reduce $\tilde{t}_c$ in CO_2-water mixtures by up to around 10% at the conditions examined in our study, but realistically not more than 20% even at very high pressures where the CO_2 solubility is relatively high.

	η	$\tilde{t}_c$	% difference for $\tilde{t}_c$	$\tilde{s}_c$	% difference for $\tilde{s}_c$
Fixed interface	0	50.2	...	0.0666	...
$c_{sat} = 0.02$	0.0114	48.9	2.6	0.0663	0.5
$c_{sat} = 0.043$	0.0246	47.4	5.6	0.0658	1.2
$c_{sat} = 0.06$	0.0346	46.3	7.8	0.0655	1.7
$c_{sat} = 0.08$	0.0465	44.9	10.6	0.0651	2.3
$c_{sat} = 0.10$	0.0586	43.6	13.2	0.0647	2.9
$c_{sat} = 0.12$	0.0709	42.3	15.7	0.0643	3.5
$c_{sat} = 0.14$	0.0834	40.9	18.5	0.0638	4.2

time to $\tilde{c}_{\text{base}}$ when the interface remains fixed is $1/[1 + \text{erf}(\eta)]$. This ratio is less than one and monotonically decreases with η for $\eta > 0$. Thus, movement of the interface reduces the magnitude of $\tilde{c}_{\text{base}}$ because the increase in volume dilutes the CO_2 concentration in the liquid phase. This translates to a reduction in the density ρ and an increase in the critical time. However, the volume expansion also increases the thickness of the dense, CO_2-dissolved liquid layer near the interface. The increased thickness destabilizes the base state and allows the onset of convection to occur earlier. Previous studies[11,16] have found that onset of convection cannot occur when the Rayleigh number Ra is less than about 30. Since Ra appears in location of the bottom boundary, this value of Ra represents the minimum height of the porous domain necessary for onset to occur. Slim and Ramakrishan[16] reason that the vertical confinement when $\text{Ra} < 30$ impedes the growth of small wavenumber modes and prevents the formation of large-scale convection cells. We offer a different interpretation. We believe that $\text{Ra} \approx 30$ represents a critical thickness of the CO_2-dissolved liquid layer. When the thickness of the layer is less than this critical value (i.e., when only a small amount of CO_2 has dissolved in the liquid phase), the buoyancy-driven instabilities are insufficiently strong to overcome the dissipation of the perturbations due to diffusion. The base state does not become unstable in such a case.

The onset of convection occurs earlier when the interface moves because the relative increase in the thickness is greater than the decrease in ρ. To show this, we examine the average mass density $\langle\rho\rangle$, which is the value obtained by spatially averaging ρ in all directions. It is equal to

$$\langle\rho\rangle = \rho_0(1 + \alpha\langle c\rangle) = \rho_0(1 + \alpha\langle c_{\text{base}}\rangle),$$

where the second equality follows from the fact that the perturbations do not affect the average CO_2 concentration. For illustration, we consider a binary mixture where $c_{\text{sat}} = 0.08$ and $\langle\rho\rangle - \rho_0 = 0.01\rho_0$. We have $\eta = 0.0465$ and $1/[1 + \text{erf}(\eta)] = 0.95$ for this value of c_{sat}, and find that

$$\frac{\langle\rho\rangle_{\text{moving}}}{\langle\rho\rangle_{\text{fixed}}} = \frac{\rho_0(1 + 0.0095)}{\rho_0(1 + 0.01)} = 0.9995.$$

Interface movement decreases the average density by only 0.05%. Using the value of the Rayleigh number from the preceding paragraph, the relative increase in the thickness of the CO_2-dissolved layer may be estimated as $\tilde{h}(\tilde{t}_c)/30$. For $\tilde{t}_c = 44.9$, we have

$$\frac{\tilde{h}(44.9)}{30} = \frac{2(0.0465)\sqrt{44.9}}{30} = 0.021.$$

Therefore, the relative increase in thickness may be over an order of magnitude greater than the decrease in $\langle\rho\rangle$. In reality, the decrease in $\langle\rho\rangle$ may be even less than the value calculated in our example. As mentioned in Sec. II A, the maximum density increase $\Delta\rho$ may be as high as about $0.02\rho_0$ for CO_2-water mixtures, and several percent of ρ_0 for CO_2-hydrocarbon mixtures. The onset of convection occurs well before the liquid phase becomes saturated with CO_2 at the equilibrium concentration. Thus, $\langle\rho\rangle - \rho_0 \ll \Delta\rho$, and the ratio $\langle\rho\rangle_{\text{moving}}/\langle\rho\rangle_{\text{fixed}}$ will be closer to unity than in our example.

For the reasons discussed at the end of Sec. II D, we are unable to perform a stability analysis for high CO_2 solubility hydrocarbons where c_{sat} may be as large as 50 mass percent and swelling can be as much as 60%. Nevertheless, the trends in our results strongly suggest that the decrease in the critical time may be much more pronounced in hydrocarbons than in water. It may be comparable to the decrease in the critical time due to permeability anisotropy, which we have studied in our previous paper.[24] This could have important implications for CO_2 improved oil recovery.

IV. CONCLUSIONS

We have performed linear stability analyses to study the effect of fluid compressibility and interface movement on the onset of buoyancy-driven convection in porous media. Our work has

applications to both CO_2 improved oil recovery and CO_2 sequestration, although we have focused mainly on the latter. We draw the following conclusions:

- Compressibility, which is related to a non-zero divergence of the velocity field, has a negligible effect on the onset of convection in CO_2-water mixtures. The critical time and critical wavenumber for an incompressible vs. compressible fluid are virtually the same.
- There are two contributions to the divergence of the velocity field: (1) a change in the volume and (2) a change in the mass. The two contributions are comparable in magnitude for CO_2-water mixtures and largely cancel each other. This explains why compressibility has a negligible effect, and it also suggests that the volume change from CO_2 dissolution may be significant. The volume change is manifested in the form of a moving interface between the CO_2 phase and the liquid (aqueous or hydrocarbon) phase.
- Interface movement may reduce the critical time by up to around 10% in CO_2-water mixtures. The critical wavenumber also decreases, but to a lesser extent. A 10% reduction in the critical time can be significant in low permeability media, where it could represent a time period of several months or even years.
- The base state becomes more buoyantly unstable because interface movement increases the thickness of the dense, CO_2-dissolved liquid layer near the interface. The end result is that the onset of convection occurs earlier.
- The effect of a moving interface may be much more pronounced in hydrocarbons than in water. This could have important implications for CO_2 improved oil recovery.

ACKNOWLEDGMENTS

Financial support for this work has been provided by the member companies of the Reservoir Engineering Research Institute.

[1] "World energy outlook 2011," Technical Report No. 61 2011 24 1P1, edited by F. Birol, L. Cozzi, A. Bromhead, J. Corben, M. Baroni, T. Gould, P. Olejarnik, D. Dorner, R. Priddle, and M. van der Hoeven (Directorate of Global Energy Economics of the International Energy Agency, Paris, 2011).
[2] A. Firoozabadi and P. Cheng, "Prospects for subsurface CO_2 sequestration," AIChE J. **56**, 1398–1405 (2010).
[3] T. Ahmed, H. Nasrabadi, and A. Firoozabadi, "Complex flow and composition path in CO_2 injection schemes from density effects," Energy Fuels **26**, 4590–4598 (2012).
[4] G. J. Weir, S. P. White, and W. M. Kissling, "Reservoir storage and containment of greenhouse gases," Transp. Porous Med. **23**, 37–60 (1996).
[5] E. Lindeberg and D. Wessel-Berg, "Vertical convection in an aquifer column under a gas cap of CO_2," Energy Convers. Manage. **38**, S229 (1997).
[6] "IPCC special report on carbon dioxide capture and storage," Technical Report, edited by B. Mertz, O. Davidson, H. de Doninck, M. Loos, and L. Meyer (Working Group III of the Intergovernmental Panel on Climate Change, Cambridge University Press, Cambridge, 2005).
[7] S. J. Ashcroft and M. Ben Isa, "Effect of dissolved gases on the densities of hydrocarbons," J. Chem. Eng. Data **42**, 1244–1248 (1997).
[8] J. Ennis-King and L. Paterson, "Role of convective mixing in the long-term storage of carbon dioxide in deep saline formations," SPE J. **10**, 349–356 (2005).
[9] J. R. Johnston, "Weeks Island gravity stable CO_2 pilot," in *Proceedings of the SPE Enhanced Oil Recovery Symposium, Tulsa, OK, USA, 1988* (The Society of Petroleum Engineers (SPE), 1988), p. 17351.
[10] V. K. Bangia, F. F. Yau, and G. R. Hendricks, "Reservoir performance of a gravity-stable, vertical CO_2 miscible flood: Wolfcamp Reef Reservoir, Wellman Unit," SPE Reservoir Eng. **8**, 261–269 (1993).
[11] J. Ennis-King, I. Preston, and L. Paterson, "Onset of convection in anisotropic porous media subject to a rapid change in boundary conditions," Phys. Fluids **17**, 084107 (2005).
[12] X. Xu, S. Chen, and D. Zhang, "Convective stability analysis of the long-term storage of carbon dioxide in deep saline aquifers," Adv. Water Resour. **29**, 397–407 (2006).
[13] A. Riaz, M. Hesse, H. A. Tchelepi, and F. M. Orr, "Onset of convection in a gravitationally unstable diffusive boundary layer in porous media," J. Fluid Mech. **548**, 87–111 (2006).
[14] H. Hassanzadeh, M. Pooladi-Darvish, and D. W. Keith, "Stability of a fluid in a horizontal saturated porous layer: Effect of non-linear concentration profile, initial, and boundary conditions," Transp. Porous Med. **65**, 193–211 (2006).
[15] S. Rapaka, S. Chen, R. J. Pawar, P. H. Stauffer, and D. Zhang, "Non-modal growth of perturbations in density-driven convection in porous media," J. Fluid Mech. **609**, 285–303 (2008).
[16] A. C. Slim and T. S. Ramakrishan, "Onset and cessation of time-dependent, dissolution-driven convection in porous media," Phys. Fluids **22**, 124103 (2010).

[17] H. Hassanzadeh, M. Pooladi-Darvish, and D. W. Keith, "The effect of natural flow of aquifers and associated dispersion on the onset of buoyancy-driven convection in a saturated porous medium," AIChE J. **55**, 475–485 (2009).
[18] M. Javaheri, J. Abedi, and H. Hassanzadeh, "Linear stability analysis of double-diffusive convection in porous media, with application to geological storage of CO_2," Transp. Porous Med. **84**, 441–456 (2010).
[19] M. Bestehorn and A. Firoozabadi, "Effect of fluctuations on the onset of density-driven convection in porous media," Phys. Fluids **24**, 114102 (2012).
[20] J. Ennis-King and L. Paterson, "Coupling of geochemical reactions and convective mixing in the long-term geological storage of carbon dioxide," Int. J. Greenhouse Gas Control **1**, 86–93 (2007).
[21] K. Ghesmat, H. Hassanzadeh, and J. Abedi, "The impact of geochemistry on convective mixing in a gravitationally unstable diffusive boundary layer in porous media: CO_2 storage in saline aquifers," J. Fluid Mech. **673**, 480–512 (2011).
[22] J. S. Hong and M. C. Kim, "Effect of anisotropy of porous media on the onset of buoyancy-driven convection," Transp. Porous Med. **72**, 241–253 (2008).
[23] S. Rapaka, R. J. Pawar, P. H. Stauffer, D. Zhang, and S. Chen, "Onset of convection over a transient base-state in anisotropic and layered porous media," J. Fluid Mech. **641**, 227–244 (2009).
[24] P. Cheng, M. Bestehorn, and A. Firoozabadi, "Effect of permeability anisotropy on buoyancy-driven flow for CO_2 sequestration in saline aquifers," Water Resour. Res. **48**, W09539, doi:10.1029/2012WR011939 (2012).
[25] H. Hassanzadeh, M. Pooladi-Darvish, and D. W. Keith, "Scaling behavior of convective mixing, with application to geological storage of CO_2," AIChE J. **53**, 1121–1131 (2007).
[26] J. J. Hidalgo and J. Carrera, "Effect of dispersion on the onset of convection during CO_2 sequestration," J. Fluid Mech. **640**, 441–452 (2009).
[27] G. S. H. Pau, J. B. Bell, K. Pruess, A. S. Almgren, M. J. Lijewski, and K. Zhang, "High-resolution simulation and characterization of density-driven flow in CO_2 storage in saline aquifers," Adv. Water Resour. **33**, 443–455 (2010).
[28] J. T. H. Andres and S. S. S. Cardoso, "Onset of convection in a porous medium in the presence of chemical reaction," Phys. Rev. E **83**, 046312 (2011).
[29] M. T. Elenius and K. Johannsen, "On the time scales of nonlinear instability in miscible displacement porous media flow," Comput. Geosci. **16**, 901–911 (2012).
[30] R. Farajzadeh, H. Salimi, P. L. J. Zitha, and H. Bruining, "Numerical simulation of density-driven natural convection in porous media with application for CO_2 injection projects," Int. J. Heat Mass Transfer **50**, 5054–5064 (2007).
[31] T. Kneafsey and K. Pruess, "Laboratory flow experiments for visualizing carbon dioxide-induced, density-driven brine convection," Transp. Porous Med. **82**, 123–139 (2010).
[32] R. Nazari Moghaddam, B. Rostami, P. Pourafshary, and Y. Fallahzadeh, "Quantification of density-driven natural convection for dissolution mechanism in CO_2 sequestration," Transp. Porous Med. **92**, 439–456 (2012).
[33] Z. Li and A. Firoozabadi, "Cubic-plus-association equation of state for water-containing mixtures: Is "cross association" necessary?" AIChE J. **55**, 1803–1813 (2009).
[34] B. Meulenbroek, R. Farajzadeh, and H. Bruining, "The effect of interface movement and viscosity variation on the stability of a diffusive interface between aqueous and gaseous CO_2," Phys. Fluids **25**, 074103 (2013).
[35] R. M. Lansangan and J. L. Smith, "Viscosity, density, and composition measurements of CO_2/West Texas oil systems," SPE Reservoir Eng. **8**, 175–182 (1993).
[36] T. D. Foster, "Stability of a homogeneous fluid cooled uniformly from above," Phys. Fluids **8**, 1249–1257 (1965).
[37] A. Firoozabadi, *Thermodynamics of Hydrocarbon Reservoirs* (McGraw-Hill, New York, 1999).
[38] J. Moortgat, Z. Li, and A. Firoozabadi, "Three-phase compositional modeling of CO_2 injection by higher-order finite element methods with CPA equation of state for aqueous phase," Water Resour. Res. **48**, W12511, doi:10.1029/2011WR011736 (2012).
[39] J. C. Slattery, *Advanced Transport Phenomena* (Cambridge University Press, Cambridge, 1999).
[40] L. G. Leal, *Advanced Transport Phenomena: Fluid Mechanics and Convective Transport Processes* (Cambridge University Press, Cambridge, 2007).
[41] K. B. Haugen and A. Firoozabadi, "Composition at the interface between multicomponent non-equilibrium fluid phases," J. Chem. Phys. **130**, 064707 (2009).
[42] J. Crank, *Free and Moving Boundary Problems* (Oxford University Press, Oxford, 1987).
[43] J. Crank, *Mathematics of Diffusion*, 2nd ed. (Oxford University Press, Oxford, 1980).
[44] H. S. Carslaw and J. C. Jaeger, *Conduction of Heat in Solids*, 2nd ed. (Oxford University Press, Oxford, 1986).
[45] S. Takenouchi and G. C. Kennedy, "The binary system H_2O-CO_2 at high temperatures and pressures," Am. J. Sci. **262**, 1055–1074 (1964).
[46] A. E. Mather and E. U. Franck, "Phase equilibria in the system carbon dioxide-water at elevated pressures," J. Phys. Chem. **96**, 6–8 (1992).
[47] R. Farajzadeh, H. A. Delil, P. L. J. Zitha, and J. Bruining, "Enhanced mass transfer of CO_2 into water and oil by natural convection," in *Proceedings of the SPE Europec/EAGE Annual Conference and Exhibition, London, UK, 2007* (The Society of Petroleum Engineers (SPE), 2007), p. 107380.